Am J Nucl Med Mol Imaging 2022;12(1):15-24
www.ajnmmi.us /ISSN:2160-8407/ajnmmi0139814

Original Article

A new solid target design for the production of ^{89}Zr and radiosynthesis of high molar activity [^{89}Zr]Zr-DBN

Mukesh K Pandey[1*], Aditya Bansal[1*], Jason R Ellinghuysen[1], Daniel J Vail[1], Heather M Berg[1], Timothy R DeGrado[1,2]

[1]Division of Nuclear Medicine, Department of Radiology, Mayo Clinic Rochester, MN 55906, USA; [2]Department of Radiology, University of Colorado Anschutz Medical Campus, Aurora, CO 80045, USA. [*]Equal contributors.

Received October 13, 2021; Accepted November 22, 2021; Epub February 15, 2022; Published February 28, 2022

Abstract: Due to the advent of various biologics like antibodies, proteins, cells, viruses, and extracellular vesicles as biomarkers for disease diagnosis, progression, and as therapeutics, there exists a need to have a simple and ready to use radiolabeling synthon to enable noninvasive imaging trafficking studies. Previously, we reported [^{89}Zr] zirconium-*p*-isothiocyanatobenzyl-desferrioxamine ([^{89}Zr]Zr-DBN) as a synthon for the radiolabeling of biologics to allow PET imaging of cell trafficking. In this study, we focused on improving the molar activity (A_m) of [^{89}Zr]Zr-DBN, by enhancing ^{89}Zr production on a low-energy cyclotron and developing a new reverse phase HPLC method to purify [^{89}Zr]Zr-DBN. To enhance ^{89}Zr production, a new solid target was designed, and production yield was optimized by varying, thickness of yttrium foil, beam current, irradiation duration and proton beam energy. After optimization, 4.78±0.33 GBq (129.3±8.9 mCi) of ^{89}Zr was produced at 40 μA for 180 min (3 h) proton irradiation decay corrected to the end of bombardment with a saturation yield of 4.56±0.31 MBq/μA. Additionally, after reverse phase HPLC purification the molar activity of [^{89}Zr]Zr-DBN was found to be in 165-316 GBq/μmol range. The high molar activity of [^{89}Zr]Zr-DBN also allowed radiolabeling of low concentration of proteins in relatively higher yield. The stability of [^{89}Zr]Zr-DBN was measured over time with and without the presence of ascorbic acid. The newly designed solid target assembly and HPLC method of [^{89}Zr]Zr-DBN purification can be adopted in the routine production of ^{89}Zr and [^{89}Zr]Zr-DBN, respectively.

Keywords: ^{89}Zr, cyclotron targetry, solid target, yttrium foil, [^{89}Zr]Zr-DBN, antibody (IgG)

Introduction

^{89}Zr has emerged as a preferred positron emission tomography (PET) isotope for the radiolabeling of various antibodies, viruses, cells, exosomes, extracellular vesicles (EVs) and nanoparticles (NPs) due to its long half-life (78.4 h) and suitable PET imaging characteristics (β^+_{max} 0.9 MeV, 22.7%) [1-4]. To provide a stable labeling strategy, the macromolecules are normally covalently conjugated with a suitable chelator by using primary amines, hydroxyls or carboxylic groups present on the molecules [5]. During the conjugation reaction, appropriately functionalized (activated esters, isothiocyanates, reactive ketones and other easily reactive functional groups) chelators are used in excess (typically 3-6 fold) as compared to the biologics/macromolecules to ensure adequate availability of the chelators on the biologics/macromolecules post-conjugation to enable efficient radiolabeling with ^{89}Zr [6-13]. The molar activity (A_m) of the final radiolabeled biologic/macromolecule depends on the initial starting radioactivity, molar activity of the ^{89}Zr, radiolabeling yield and amount (mmol or mg) of the biologics/macromolecules present in the final formulation. To achieve high molar activity (A_m), a high concentration of ^{89}Zr radioactivity (MBq/μL) is needed, so that only a small mass (μg or ng range) of biologics/macromolecules can be used for an efficient radiolabeling, otherwise more mass of the biologics/macromolecules will be needed to compensate for the dilution caused by the higher volume of radioactivity. The production of ^{89}Zr from the cyclotron has been well documented using both liquid targets and solid targets [8-10, 13]. Among the various reported methods of ^{89}Zr production from solid targets, yttrium foil, yttrium-sputter-

Table 1. Estimation of effective beam energy at different thickness of degrader foil (aluminum) using TRIM program

Aluminum (Al) thickness (mm)	Effective Thickness (mm) with a 30-degree target	Degraded energy (MeV)
0.1	0.2	15.2
0.2	0.4	13.9
0.3	0.6	12.3

ing, yttrium-pellet and yttrium deposition are commonly known [8, 11, 12]. In this study, we aimed to improve the radiolabeling yield of ^{89}Zr labeled biologics/macromolecules by designing a new solid target for increasing the production levels of ^{89}Zr using yttrium-foil on a low-energy cyclotron and by developing a new method of purification of [^{89}Zr]zirconium-*p*-isothiocyanatobenzyl-desferrioxamine ([^{89}Zr]Zr-DBN [2, 3]) as a ready to use radiolabeling synthon for the direct radiolabeling of the biologics/macromolecules with a high molar activity [^{89}Zr]Zr-DBN.

Materials and methods

Targetry details

A PETtrace cyclotron (GE HealthCare, Waukesha, WI) was used in this study. To perform Zr-89 production, an Advanced Cyclotron Systems Inc. (ACSI) target holder was used and placed after the switching magnet at a 30 degree angle with respect to beamline on a PETtrace cyclotron; the proton beam energy was degraded using 0.1, 0.2, and 0.3 mm aluminum foils to ~15.2, 13.9 and 12.3 MeV, respectively, as estimated from TRIM program (**Table 1**). A new target assembly was designed (**Figure 1**) to simply accommodate degrader foil (aluminum foil), target foil (Yttrium foil), and back plate (aluminum plate, 2.0 mm) with water cooling at the back plate and helium cooling to the front. Variable thickness (0.1 mm and 0.127 mm) of yttrium foils were purchased from the Alfa-Aesar (50×50 mm, 99.9%) Haverhill, MA, USA.

Chemicals

The trace metal grade concentrated nitric acid (67-70% as HNO_3) and hydrochloric acid (34-37% as HCl) were purchased from the Fisher Chemicals part of the Thermo Fisher Scientific (Waltham MA). Sodium bicarbonate, acetonitrile (HPLC grade) and trifluoroacetic acid (TFA, 99%) were purchased from Sigma-Aldrich (St. Louis, MO). The hydroxamate resin was synthesized in-house as previously described by the Pandey et al. [10]. The i-TLC paper was purchased from Agilent Technologies (Palo Alto, CA). The labeling precursor p-SCN-Bn-Deferoxamine (B-705, ≥94%) was purchased from Macrocyclics, Plano, TX. Deionized water was obtained from Barnstead Nanopure water purification system from Thermo Fisher Scientific, Waltham, MA.

Instrumentation

The radioactive samples were counted using a Wizard 2480 gamma counter (Perkin Elmer, Waltham, MA). Radionuclidic purity was evaluated using a high-purity germanium gamma spectrometer (Canberra, Meriden, CT) running Genie 2000 software. The radioactivity readings were recorded using a CRC dose calibrator (489 setting for ^{89}Zr and 465 for ^{88}Y, CRC-55tPET, Capintec, Ramsey, NJ).

Purification of cyclotron produced ^{89}Zr and radiosynthesis of [^{89}Zr]Zr-DBN

The cyclotron produced ^{89}Zr was purified following previously reported methods [8-10]. The purified [^{89}Zr]Zr-oxalate was converted to [^{89}Zr]Zr-chloride using anion exchange column Chromafix 30-PS-HCO_3 SPE 45 mg cartridge (Macherey-Nagel, Düren, Germany) following Larenkov et al.'s method [14]. The cartridge was activated with a 6.0 mL acetonitrile followed by 10 mL saline and 10 mL deionized water wash with air drying steps in between each solvent. The ^{89}Zr was trapped on an activated Chromafix 30-PS-HCO_3 SPE (45 mg) cartridge and oxalate was removed with 50 mL deionized water. Finally, ^{89}Zr was eluted as [^{89}Zr]Zr-chloride with 0.5 mL 1 N HCl in a 97.4±1.1 (n=10) elution efficiency. The eluted [^{89}Zr]Zr-chloride was then dried using a concentrator (Savant™ SpeedVac™ High Capacity Concentrator, Thermo Fisher Scientific Inc., Logan, UT) at 0.42 torr and 65°C. The dried [^{89}Zr]Zr-chloride was resuspended in ~180 µL of 0.1 N HCl and then neutralized to pH ~8.0 with ~18 µL 1 M Na_2CO_3. To this, 2.5 mM DFO-Bz-NCS in DMSO (Macrocylics, Plano TX) was added to give a final concentration of ~54 µM DFO-Bz-NCS, and chelation of ^{89}Zr proceeded at 37°C for

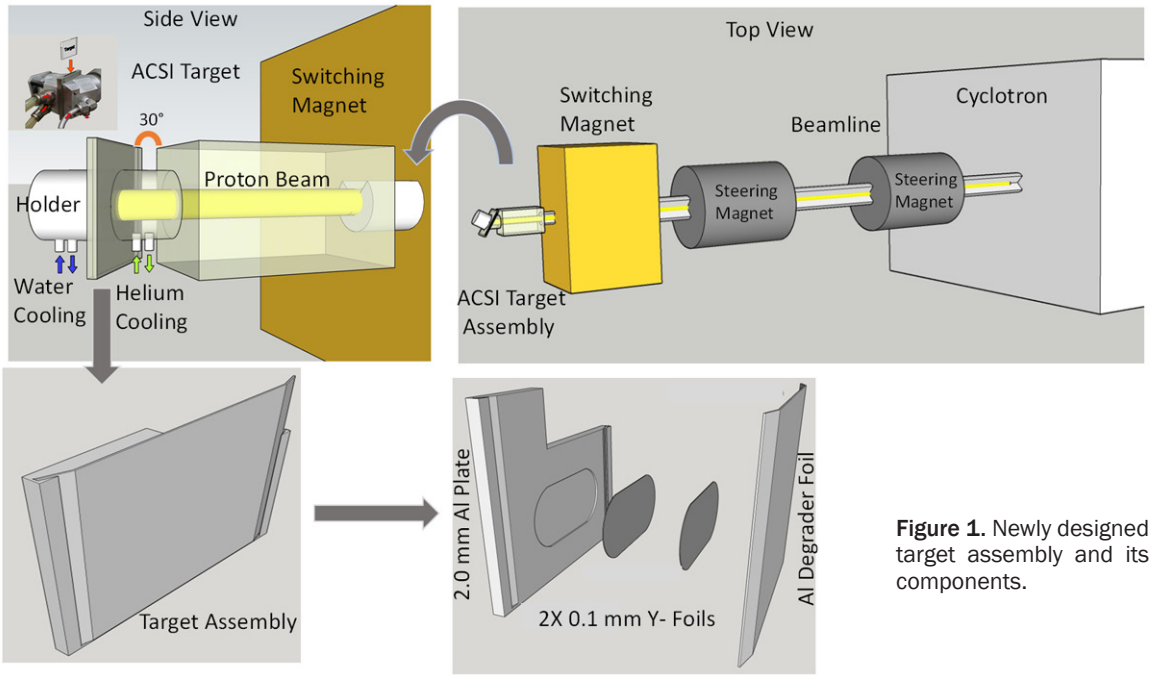

Figure 1. Newly designed target assembly and its components.

~30 min in a thermomixer at 550 rpm. The chelation efficiency was determined by silica gel iTLC (Agilent Technologies Inc., Santa Clara, CA) with 100 mM DTPA pH 7 as the mobile phase. [^{89}Zr]Zr-DBN showed an R_f=0, whereas [^{89}Zr]Zr-chloride had an R_f=0.9 (Figure S1).

HPLC purification of [^{89}Zr]Zr-DBN

The [^{89}Zr]Zr-DBN reaction mixture was diluted to ~1.0 mL with deionized water (neutralized with sodium carbonate to final pH 7.0) before HPLC purification. The purification was performed at room temperature using a reverse phase Agilent Zorbax 300-SB-C-18 (5 µm; 9.4×250 mm) column (Agilent Technologies Inc., Santa Clara, CA) and 1.0 mL injection loop size. The gradient elution was performed with solvent A (deionized H_2O +0.1% TFA) and solvent B (Acetonitrile +0.1% TFA). The flow rate was set at 1.8 mL/min and absorbance was set at 220 nm. The purification was performed using 0-5 min (static 5% solvent B), 5-10 min (gradient, 5-34% solvent B), 10-95 min (gradient, 34-41.5% solvent B), 95-100 min (gradient, 41.5-85% solvent B), 100-110 min (gradient, 85-5% solvent B) and 110-115 min (static, 5% solvent B) gradient program. The total separation time was ~35 min. Blank runs were performed in between the sample injections. Concentration of nonradioactive (UV) Zr-DBN was estimated using a calibration curve (Figure S2).

Radiolabeling of antibody with purified [^{89}Zr]Zr-DBN

The purified [^{89}Zr]Zr-DBN (~7.2 mL) was collected at the appropriate retention time in a glass test tube and dried using the concentrator at 0.42 torr and at room temperature. For radiolabeling of an example antibody, different concentrations (0.1, 0.5 and 1.0 mg/mL) of human IgG were prepared in phosphate buffered saline (PBS) from a stock solution (~10 mg/mL) of ChromPure Human IgG, whole molecule (Jackson Immuno Research Inc., West Grove, PA). The pH of the different human IgG solutions was adjusted to pH 9.0 using appropriate volumes of 0.5 M Na_2CO_3. Immediately after adjusting the pH, 200 µL of pH adjusted human IgG solution was added to ~3.7 MBq of [^{89}Zr]Zr-DBN. The final pH was adjusted with additional volumes of 0.5 M Na_2CO_3 to achieve a pH of 9.0. The IgG radiolabeling reaction was performed at 37°C for ~30 min in a thermomixer at 550 rpm. After 30 min of reaction, the extent of radiolabeling was quantified using silica gel iTLC (Agilent Technologies Inc., Santa Clara, CA, USA) with 20 mM citric acid (pH 4.9-5.1): methanol (1:1, V:V) as the mobile phase. On iTLC, the [^{89}Zr]Zr-DBN-IgG showed an R_f=0.0, where-

as [^{89}Zr]Zr-chloride and [^{89}Zr]Zr-DBN had an R_f=0.99 (Figures S3, S4 and S5).

Stability of purified [^{89}Zr]Zr-DBN

The purified and concentrated [^{89}Zr]Zr-DBN was stored at -20°C and stability was tested at 0 h, 24 h and 72 h post HPLC purification and concentration in comparison with unpurified [^{89}Zr]Zr-DBN which was also stored at -20°C. To test the stability, the frozen [^{89}Zr]Zr-DBN was allowed to come to room temperature and reconstituted with ~100 µL DMSO. The reconstituted [^{89}Zr]Zr-DBN (~3.7 MBq) was diluted with ~900 µL neutralized deionized water (pH 7.0) and pH was further adjusted to pH 7.0 using 1 M Na_2CO_3. The stability of reconstituted and neutralized [^{89}Zr]Zr-DBN was tested using the same HPLC method that was used for [^{89}Zr]Zr-DBN purification.

Effect of ascorbic acid on stability of purified [^{89}Zr]Zr-DBN

The HPLC purified [^{89}Zr]Zr-DBN (~7.2 mL) was divided into two equal parts of ~3.6 mL each. In one-part, 25 µL of 200 mg/mL ascorbic acid (Sigma Aldrich, St. Louis, MO) was added. Both ascorbic acid treated, and untreated fractions were concentrated at 0.42 torr and room temperature. The concentrated solutions were stored at -20°C and stability was tested at 0 h, 24 h and 48 h using the same HPLC method used for [^{89}Zr]Zr-DBN purification.

Measurement of trace metal impurity and radionuclidic impurities

The presence of various (Y, Fe, Al) trace metals in the purified samples were analyzed using inductively coupled Plasma spectrometer using PerkinElmer Elan or PerkinElmer NexION 350D ICP-MS spectrometers (Waltham MA) equipped with Elemental Scientific Inc. (ESI) SC2-DX autosamplers (Omaha NE). The mass spectrometers were equipped with ESI microflow PFA-ST nebulizers and quartz cyclonic spray chambers including a baffle. Radionuclidic purity was measured via high purity germanium gamma spectrometer (HPGe). Purified [^{89}Zr]Zr-oxalate samples were counted in a dose calibrator (at Zr-89 setting, 489) and analyzed by HPGe, at different time points over the period of 3-4 months from the day of purification to estimate the presence of ^{88}Zr ($T_{1/2}$ 83.4 days) due to possible ^{89}Y(p, 2n)^{88}Zr reaction and its daughter radionuclide ^{88}Y ($T_{1/2}$ 106.6 days) in the final formulation (Figure S6A-C). Using the manufacturer's ionization response versus gamma energy of the dose calibrator (Capintec/Mirion, Florham Park, NJ), the radioactivities of ^{88}Zr and ^{88}Y were estimated at time of measurement, and decay corrected to estimate ^{88}Zr produced at EOB.

Statistical analysis

All values are given as mean ± standard deviation. Statistical significance of differences was determined by two-tailed student's T-test. *P* values <0.05 were considered statistically significant.

Results and discussion

New target design and production of ^{89}Zr from cyclotron using solid target

To enhance our cyclotron production of capability of ^{89}Zr, we switched our production method from liquid target to solid target [9, 10]. For the simplicity of ^{89}Zr production, we chose to use a yttrium foil as a target material. In this new target design, there are three major components, (i) aluminum degrader (0.2 mm) to degrade the proton-beam to ~13.9 MeV, (ii) aluminum back plate (2.0 mm) for housing yttrium foils and water cooling and (iii) two yttrium foils (0.1 mm each) stacked on each other. On the back plate, there is an oval shaped recess to house two yttrium foils (0.1 mm each). In addition, the back-aluminum plate also has grooves on both the sides to allow the front aluminum degrader foil to slide in to complete the intact target assembly (**Figure 1**). The "L" shape of the back-aluminum plate was deliberately designed to allow space to hold and separate it from the degrader foil after irradiation. After designing a prototype target assembly, we noticed a very small amount of paper glue is needed outside the beam strike area to adhere both the yttrium foils together along with the back plate. The amount of glue did not impede separation of the yttrium foils after irradiation. To optimize ^{89}Zr production yield, we tested various thicknesses of yttrium foil (0.1-0.25 mm), different beam current (25-40 µA) and different irradiation durations (120-180 min). The optimized production yields are listed in **Table 2**. We

Table 2. Optimized cyclotron production of ^{89}Zr using a new target design

Beam current (μA)	Irradiation time (min)	Yttrium foil thickness (mm)	Corrected yield at EOB* (mCi)	Corrected yield at EOB (MBq)	Saturation yield (GBq/μA)
25-30 (n=6)	120	0.1	27.1±7.8	1001±288	2.07±0.60
40 (n=8)	120	0.25	91.8±16.8	3396±620	4.84±0.88
40 (n=19)	180	0.2	129.±8.9	4784±330	4.56±0.31

*EOB: End of bombardment.

Table 3. Comparison of ^{89}Zr production yield at different proton beam energies and associated coproduction of ^{88}Zr (^{88}Zr decayed to ^{88}Y)

Beam Energy (MeV)	Aluminum degrader foil thickness (mm)	Beam current (μA)	Irradiation time (min)	Yttrium foil thickness (mm)	Corrected yield at EOB* (mCi)	Corrected yield at EOB (GBq)	Saturation yield (GBq/μA)	% of ^{88}Zr (^{88}Y)
15.2	0.1	40 (n=19)	180	0.2	129.0±8.9	4.78±0.33	4.56±0.31	0.014±0.006
13.9	0.2	38 (n=3)	180	0.2	78.6±5.5	2.91±0.20	2.93±0.21	negligible and unquantifiable
12.3	0.3	38 (n=3)	180	0.2	56.3±2.0	2.08±0.07	2.09±0.07	None

*EOB: End of bombardment.

Table 4. Analysis of metal ions in purified ^{89}Zr using ICP-MS

Metal ions	Y	Al	Fe
Quantity (μg/mL) ± SD	0.38±0.52 (n=19)	0.07±0.06 (n=18)	0.07±0.08 (n=17)

noticed an expected 2.33-fold improvement in saturation yield from 2.07±0.60 MBq/μA to 4.84±0.88 MBq/μA on changing yttrium foil thickness from 0.1 mm to 0.25 mm along with beam current from 25-30 μA to 40 μA for a 120 min proton irradiation. To reduce overall yttrium content in our final solution, the ^{89}Zr production yield was optimized with 0.2 mm thick yttrium foil (two foils of 0.1 mm thickness) at 40 μA beam current for 180 min of irradiation. During this optimization, we found a saturation yield of 4.56±0.31 MBq/μA with radioactivity of 4.78±0.33 GBq (129.3±8.9 mCi) of ^{89}Zr, decay corrected to end of the beam. We also produced ^{89}Zr at 13.9 and 12.3 MeV proton beam energies. The production yields and radionuclide purity of ^{89}Zr were compared at different proton energies in **Table 3**. It is important to mention that when irradiation was performed on same 0.2 mm thick yttrium foil for 180 min at 15.2 MeV proton energy, we found >2-fold and 1.5-fold higher saturation yield compared to when it was performed at 12.3 MeV and 13.9 MeV, respectively, However, we reduced the beam current from 40 μA to 38 μA as a precaution to avoid any potential issue associated with thicker (0.2 mm and 0.3 mm Al) degrader foil. Following previously developed methods, irradiated yttrium foil was dissolved slowly in 2 mL of 6 N HNO_3 at room temperature. After complete dissolution, the solution was diluted with 7 mL of deionized water and loaded slowly onto the hydroxamate resin (100 mg) column. After loading, the hydroxamate resin was washed with 20 mL of 2 N HCl to remove trace quantities of yttrium salt followed by 10 mL of deionized water to remove any leftover acid before eluting ^{89}Zr with 3.0 mL of 1M oxalic acid.

The purified ^{89}Zr solution was analyzed for the presence of trace quantities of Y, Zr, Fe and Al using ICP-MS and results are summarized in **Table 4** with no unexpected levels of any of tested metal ions. In addition to metal ion impurity, we also tested the radionuclidic purity using HPGe for the presence of ^{88}Zr or its daughter nuclei ^{88}Y. As previously reported [15], higher beam energy (>13.1 MeV) allows (p,2n) reaction and produces small quantity of ^{88}Zr. Based on our analysis, we found 0.014±0.006% (n=5) of total non ^{89}Zr related radioactivity as a radionuclidic impurity at end of purification, which includes both ^{88}Zr due to potential (p,2n) reaction and ^{88}Y ($T_{1/2}$ 106.6 days) the daughter nuclei of ^{88}Zr ($T_{1/2}$ 83.4 days) (**Table 3**).

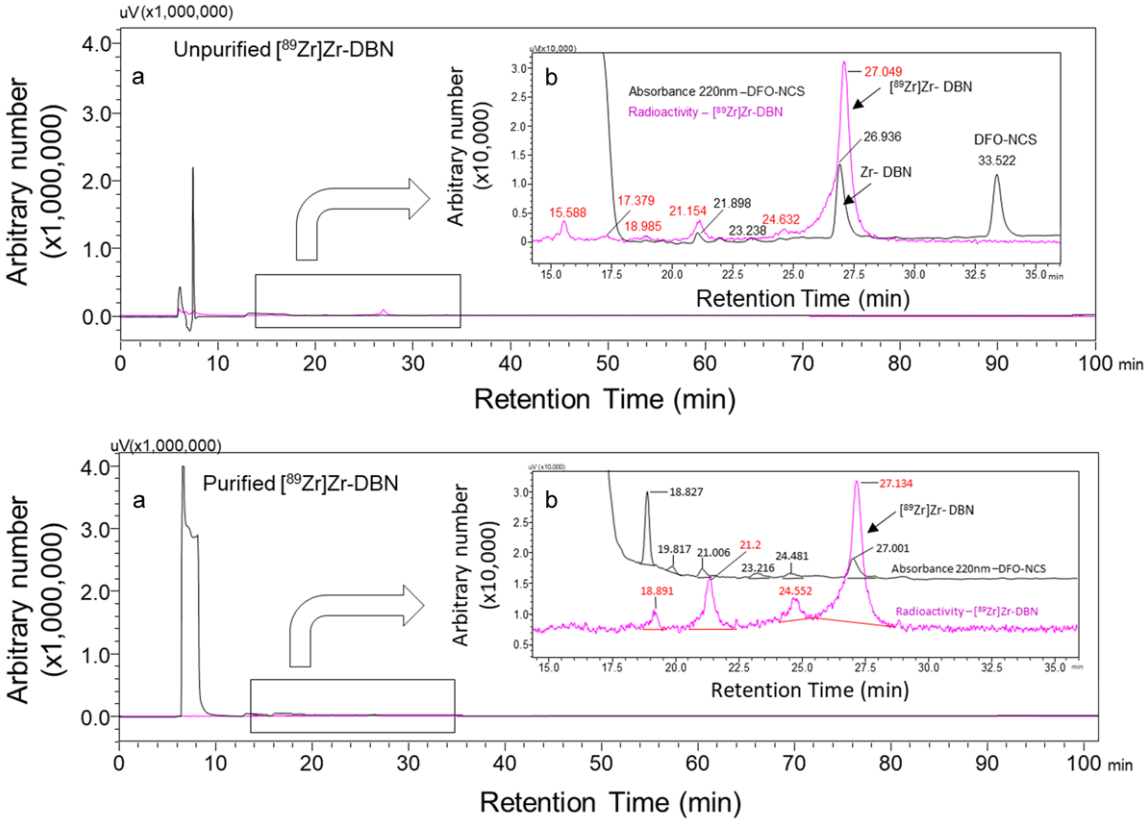

Figure 2. Comparison of HPLC traces of unpurified and purified [89Zr]Zr-DBN.

Radiosynthesis and HPLC purification of [89Zr]Zr-DBN

The [89Zr]Zr-DBN was synthesized as reported previously by reacting [89Zr]Zr-chloride (neutralized to pH ~8.0) and 10.69 nmoles of DFO-Bz-NCS in DMSO at 37°C for ~30 min. The percentage of radiolabeling was determined by silica gel iTLC using 100 mM DTPA (pH 7) as the mobile phase. Based on iTLC, radiolabeling yield was found to be >95%. In previous studies, we used unpurified [89Zr]Zr-DBN for labeling of various biologics (proteins, cells, viruses, EVs etc) but noticed some biologics (having low protein concentration) were more sensitive and gave poor radiolabeling yield with unpurified [89Zr]Zr-DBN. Therefore, in this study, we attempted to purify [89Zr]Zr-DBN to remove unlabeled p-SCN-Bn-deferoxamine (DBN) and also to increase molar activity (A_m) of [89Zr]Zr-DBN to enhance radiolabeling yield of biologics having low protein concentration with the purified [89Zr]Zr-DBN. To purify [89Zr]Zr-DBN, initially, we attempted various solid phase cartridges to separate [89Zr]Zr-DBN with DBN but in vain. We evaluated reverse phase HPLC (Zorbax 300-SB-C-18, 5 µm; 9.4×250 mm) to separate [89Zr]Zr-DBN with DBN, and after trying various solvents and their combinations, we finally settled on a gradient elution method, which was comprised of solvent A (deionized water with 0.1% TFA) and solvent B (Acetonitrile with 0.1% TFA) with a flow rate of 1.8 mL/min as described in method section. Using this newly developed HPLC method, we successfully separated [89Zr]Zr-DBN with DBN (**Figure 2**). The unlabeled DBN eluted at the retention time of 33.5 min, whereas labeled [89Zr]Zr-DBN eluted at 27.1 min, showing good separation. The [89Zr]Zr-DBN was collected and concentrated (SpeedVac) to remove acetonitrile and trifluoracetic acid before using it for the radiolabeling of the antibody/protein (IgG). The molar activities of purified and unpurified [89Zr]Zr-DBN were measured and presented in **Table 5**. It is important to mention here that the same concentration of (mg/mL) of labeling protein (IgG), starting radioactivity (mCi or MBq) of [89Zr]Zr-DBN and same labeling conditions (pH, temperature and reaction time) were used to radiolabel protein (IgG)

Table 5. Comparison of radiolabeling yield of protein (IgG) with molar activity (A_m) of purified and unpurified [89Zr]Zr-DBN

Protein concentration (mg/mL)	Molar activity of unpurified [89Zr]Zr-DBN (GBq/μmol) Average ± SD	% Radiolabeling yield of protein (IgG) With unpurified [89Zr]Zr-DBN Average ± SD	Molar activity of purified [89Zr] Zr-DBN (GBq/μmol) Average ± SD	% Radiolabeling yield of protein (IgG) with purified [89Zr]Zr-DBN Average ± SD	Average fold change in molar activity of purified over unpurified [89Zr] Zr-DBN	Average fold change in radiolabeling yield of protein (IgG) with purified over unpurified [89Zr] Zr-DBN
0.1 (n=4)	20.62±3.99	3.85±1.23	165.67±133.44	10.54±3.06*	8.0	2.7
0.5 (n=2)	24.98	11.91±0.06	316.31	28.18±0.31*	12.7	2.4
1.0 (n=3)	22.36±37.00	26.43±0.61	189.30±179.61	36.76±0.03*	8.4	1.4

*P value <0.05 with respect to unpurified [89Zr]Zr-DBN.

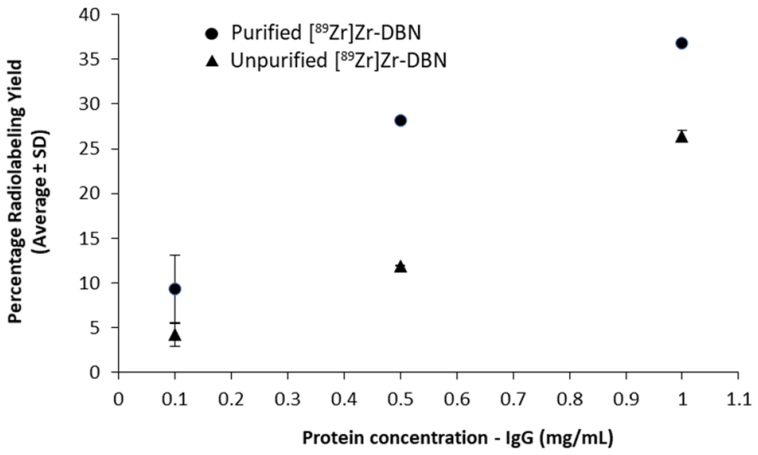

Figure 3. Comparison of radiolabeling yield of antibody (IgG) with purified and unpurified [89Zr]Zr-DBN as a function of protein (IgG) concentration.

with both purified and unpurified [89Zr]Zr-DBN. To avoid any potential confound from the starting 89Zr, we always used same batch of cyclotron produced and purified 89Zr for the synthesis of [89Zr]Zr-DBN and antibody labeling experiments with or without the [89Zr]Zr-DBN HPLC purification step.

Radiolabeling of antibody (IgG) with HPLC purified [89Zr]Zr-DBN

The radiolabeling of IgG was performed at various concentrations of antibody (0.1-1.0 mg/mL) to study radiolabeling efficiency as a function of conjugatable protein concentration. To measure the radiolabeling efficiency, we developed a new iTLC system in which both free 89Zr and unconjugated [89Zr]Zr-DBN were separated from the radiolabeled protein [89Zr]Zr-DBN-IgG. The system employs 20 mM citric acid (pH 4.9-5.1): methanol (1:1, V:V) as a mobile phase and silica gel iTLC as the solid phase. In this system, we independently confirmed the R_f's of [89Zr]Zr-chloride and [89Zr]Zr-DBN to be 0.99 (solvent front) and 0.0 (origin) for radiolabeled IgG protein ([89Zr]Zr-DBN-IgG, Figures S3, S4 and S5). The purified [89Zr]Zr-DBN gave 2.7 fold higher radiolabeling yield than unpurified [89Zr]Zr-DBN at 0.1 mg/mL concentration of protein (IgG), and a similar trend of 2.4 fold higher radiolabeling yield was noted for 0.5 mg/mL concentration of IgG protein (IgG) (**Table 5**; **Figure 3**). However, we noticed a lower impact of HPLC purification of [89Zr]Zr-DBN on radiolabeling yield for 1.0 mg/mL concentration of IgG protein (1.4 fold higher yield with purified [89Zr]Zr-DBN) (**Table 5**). These data suggest that the beneficial effect of purification of [89Zr]Zr-DBN on labeling yield is dependent on protein concentration with more benefit for labeling of biologics having low protein concentrations (**Figure 3**).

Stability of purified [89Zr]Zr-DBN overtime and effect of ascorbic acid

Encouraged by high protein (IgG) radiolabeling yield with the purified [89Zr]Zr-DBN, especially at lower protein concentrations, we thought to evaluate the radiochemical stability of [89Zr]Zr-DBN over time following HPLC purification and concentration. We noticed appearance of additional small radioactivity peaks at 18.8 min, 21.2 min and 24.5 min retention time other than the expected 27.1 min peak for the [89Zr]Zr-DBN on HPLC analysis immediately after concentrating the collected HPLC frac-

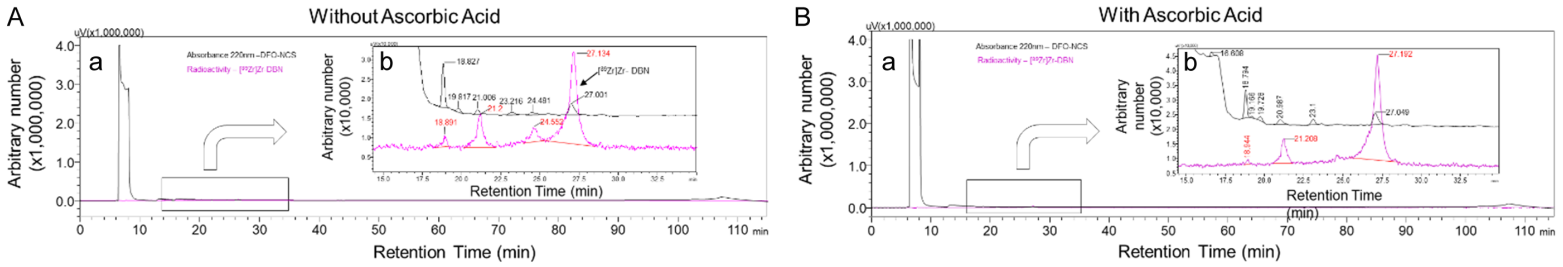

c Peak analysis table 1: Radioactivity

Radioactivity - [^{89}Zr]Zr-DBN			
Peak	RT	AUC	% AUC
1	18.891	60511	3.95
2	21.200	260559	16.99
3	24.552	121493	7.92
4 ([^{89}Zr]Zr-DBN)	**27.134**	**1090786**	**71.14**

d Peak analysis table 2: Absorbance

Absorbance 220nm – DFO-NCS			
Peak	RT	AUC	% AUC
1	18.827	138022	51.922
2	19.817	11496	4.325
3	21.006	21499	8.087
4	23.216	17587	6.616
5	24.481	12170	4.578
6 (Zr-DBN)	**27.001**	**65054**	**24.472**

c Peak analysis table 1: Radioactivity

Radioactivity - [^{89}Zr]Zr-DBN			
Peak	RT	AUC	% AUC
1	18.944	29720	1.682
2	21.208	223519	12.647
3	24.587	41564	2.352
4 ([^{89}Zr]Zr-DBN)	**27.192**	**1472567**	**83.32**

d Peak analysis table 2: Absorbance

Absorbance 220nm – DFO-NCS			
Peak	RT	AUC	% AUC
1	16.608	15497	4.498
2	18.794	110982	32.210
3	19.166	7690	2.232
4	19.728	23138	6.715
5	20.987	39456	11.451
6	23.1	35120	10.193
7 (Zr-DBN)	27.049	112674	32.701

Figure 4. Comparison of HPLC trace and peak analysis of purified [^{89}Zr]Zr-DBN with and without addition of ascorbic acid.

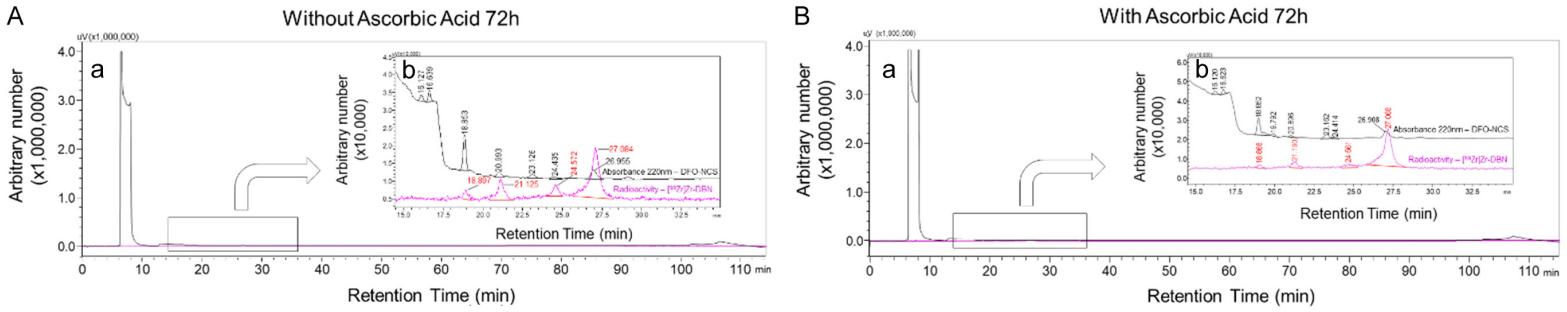

c Peak analysis table 1: Radioactivity

Radioactivity - [^{89}Zr]Zr-DBN			
Peak	RT	AUC	% AUC
1	18.897	51905	6.197
2	21.125	149667	17.870
3	24.572	81788	9.765
4 ([^{89}Zr]Zr-DBN)	27.084	554174	66.167

d Peak analysis table 2: Absorbance

Absorbance 220nm - DFO			
Peak	RT	AUC	% AUC
1	16.127	23485	7.109
2	16.639	30744	9.307
3	18.853	150760	45.638
4	20.993	23287	7.049
5	23.126	26948	8.158
6	24.435	11199	3.390
7 (Zr-DBN)	26.955	63919	19.349

c Peak analysis table 1: Radioactivity

Radioactivity - [^{89}Zr]Zr-DBN			
Peak	RT	AUC	% AUC
1	18.868	44462	4.415
2	21.190	82508	8.192
3	24.561	45948	4.562
4	27.068	834221	82.831

d Peak analysis table 2: Absorbance

Absorbance 220nm - DFO			
Peak	RT	AUC	% AUC
1	16.120	20378	6.191
2	16.623	21782	6.618
3	18.852	127442	38.721
4	19.792	16165	4.912
5	20.896	12113	3.680
6	23.162	45921	13.952
7	24.414	4796	1.457
8 (Zr-DBN)	26.908	80531	24.468

Figure 5. Comparison of HPLC trace and peak analysis of purified [^{89}Zr]Zr-DBN with and without addition of ascorbic acid at 72 h post HPLC purification.

tions for the [^{89}Zr]Zr-DBN (**Figure 4A**). Based on the retention time of the additional peaks, it was evident that none of the additional peaks resulted from demetallation of ^{89}Zr since free ^{89}Zr appears at ~6 min retention time on the HPLC analysis (Figure S7). Therefore, based on our previous experience, we suspected, it could be due to the radiation induced decomposition of [^{89}Zr]Zr-DBN [16]. Therefore, without further characterizing newly appeared peaks on HPLC, we treated the collected HPLC fraction with 25 μL of 200 mg/mL ascorbic acid before the concentration step [16]. As expected, the addition of this small quantity of ascorbic acid did help and reduced the total areas under the curve for the additional peaks present at 18.8 min, 21.2 min and 24.5 min retention times while enhancing the 27.1 min peak for [^{89}Zr]Zr-DBN by ~12% (**Figure 4B**). Addition of ascorbic improved stability of [^{89}Zr]Zr-DBN at 72 h from 66% to >82% (**Figure 5A**, **5B**). We noted that the relative percentage of radioactivity peaks in some of the fractions were not changed even after the concentration step while others showed less protection with ascorbic acid.

Conclusions

In this study, we have successfully designed and tested a new solid target assembly to produce high quantities of ^{89}Zr (4783±330 MBq, 129.3±8.9 mCi) with a saturation yield of 4.56±0.31 MBq/μA using yttrium foil via proton irradiation. In addition, we successfully developed a reverse phase HPLC method for the purification of [^{89}Zr]Zr-DBN and a new iTLC system for instant monitoring of radiolabeling yield of antibodies with [^{89}Zr]Zr-DBN. The successful production of high molar activity of [^{89}Zr]Zr-DBN has allowed 1.4-2.7 fold higher radiolabeling yield at various concentrations of antibody protein (0.1-1.0 mg/mL) in comparison to unpurified (low molar activity) [^{89}Zr]Zr-DBN. The long-term (up to 72 h) stability of purified [^{89}Zr]Zr-DBN was also studied with and without addition of ascorbic acid. The present study is a step closer to the translation of [^{89}Zr]Zr-DBN as a ready to use synthon for on-demand and on-site radiolabeling of various biologics.

Acknowledgements

This project was financially supported by the Mayo Clinic Department of Radiology, Rochester, MN 55905, the Elsie and Marvin Dekelboum family foundation and the International Atomic Energy Agency (IAEA), Vienna, Austria. Authors would also like to thank Mr. Raymond Steichen for his encouraging discussion and Dr. Shalini Sharma, and Mr. Patrick Day for their technical assistance in HPGe and ICPMS analysis, respectively.

Disclosure of conflict of interest

None.

Address correspondence to: Dr. Mukesh K Pandey, Division of Nuclear Medicine, Department of Radiology, Mayo Clinic, 200 First Street SW, Rochester, MN 55906, USA. Tel: 507-538-4221; Fax: 507-266-4461; E-mail: pandey.mukesh@mayo.edu

References

[1] Yoon JK, Park BN, Ryu EK, An YS and Lee SJ. Current perspectives on ^{89}Zr-PET imaging. Int J Mol Sci 2020; 21: 4309.

[2] Bansal A, Pandey MK, Demirhan YE, Nesbitt JJ, Crespo-Diaz RJ, Terzic A, Behfar A and DeGrado TR. Novel ^{89}Zr cell labeling approach for PET-based cell trafficking studies. EJNMMI Res 2015; 5: 19.

[3] Bansal A, Pandey MK, Yamada S, Goyal R, Schmit NR, Jeon R, Nesbitt JJ, Witt TA, Singh RD, Gunderson TM, Boroumand S, Li M, Crespo-Diaz RJ, Hillestad ML, Terzic A, Behfar A and DeGrado TR. [^{89}Zr]Zr-DBN labeled cardiopoietic stem cells proficient for heart failure. Nucl Med Biol 2020; 90-91: 23-30.

[4] Dasgupta D, Nakao Y, Mauer AS, Thompson JM, Sehrawat TS, Liao CY, Krishnan A, Lucien F, Guo Q, Liu M, Xue F, Fukushima M, Katsumi T, Bansal A, Pandey MK, Maiers JL, DeGrado T, Ibrahim SH, Revzin A, Pavelko KD, Barry MA, Kaufman RJ and Malhi H. IRE1A stimulates hepatocyte-derived extracellular vesicles that promote inflammation in mice with steatohepatitis. Gastroenterology 2020; 159: 1487-1503, e17.

[5] Bhatt NB, Pandya DN and Wadas TJ. Recent advances in zirconium-89 chelator development. Molecules 2018; 23: 638.

[6] Vosjan MJ, Perk LR, Visser GW, Budde M, Jurek P, Kiefer GE and van Dongen GA. Conjugation and radiolabeling of monoclonal antibodies with zirconium-89 for PET imaging using the bifunctional chelate p-isothiocyanatobenzyl-desferrioxamine. Nat Protoc 2010; 5: 739-43.

[7] Zeglis BM and Lewis JS. The bioconjugation and radiosynthesis of ^{89}Zr-DFO-labeled antibodies. J Vis Exp 2015: 52521.

[8] Holland JP, Sheh Y and Lewis JS. Standardized methods for the production of high specific-activity zirconium-89. Nucl Med Biol 2009; 36: 729-39.
[9] Pandey MK, Engelbrecht HP, Byrne JP, Packard AB and DeGrado TR. Production of ^{89}Zr via the ^{89}Y(p,n)^{89}Zr reaction in aqueous solution: effect of solution composition on in-target chemistry. Nucl Med Biol 2014; 41: 309-16.
[10] Pandey MK, Bansal A, Engelbrecht HP, Byrne JF, Packard AB and DeGrado TR. Improved production and processing of ^{89}Zr using a solution target. Nucl Med Biol 2016; 43: 97-100.
[11] Kasbollah A, Eu P, Cowell S and Deb P. Review on production of ^{89}Zr in a medical cyclotron for PET radiopharmaceuticals. J Nucl Med Technol 2013; 41: 35-41.
[12] Queern SL, Aweda TA, Massicano AVF, Clanton NA, El Sayed R, Sader JA, Zyuzin A and Lapi SE. Production of Zr-89 using sputtered yttrium coin targets ^{89}Zr using sputtered yttrium coin targets. Nucl Med Biol 2017; 50: 11-16.
[13] Pandey MK and DeGrado TR. Cyclotron production of PET radiometals in liquid targets: aspects and prospects. Curr Radiopharm 2021; 14: 325-339.
[14] Larenkov A, Bubenschikov V, Makichyan A, Zhukova M, Krasnoperova A and Kodina G. Preparation of zirconium-89 solutions for radiopharmaceutical purposes: interrelation between formulation, radiochemical purity, stability and biodistribution. Molecules 2019; 24: 1534.
[15] Alnahwi AH, Tremblay S and Guerin B. Comparative study with ^{89}Y-foil and ^{89}Y-pressed targets for the production of ^{89}Zr. Appl Sci 2018; 8: 1579.
[16] Pandey MK, Jacobson MS, Groth EK, Tran NG, Lowe VJ and DeGrado TR. Radiation induced oxidation of [^{18}F]fluorothia fatty acids under cGMP manufacturing conditions. Nucl Med Biol 2020; 80-81: 13-23.

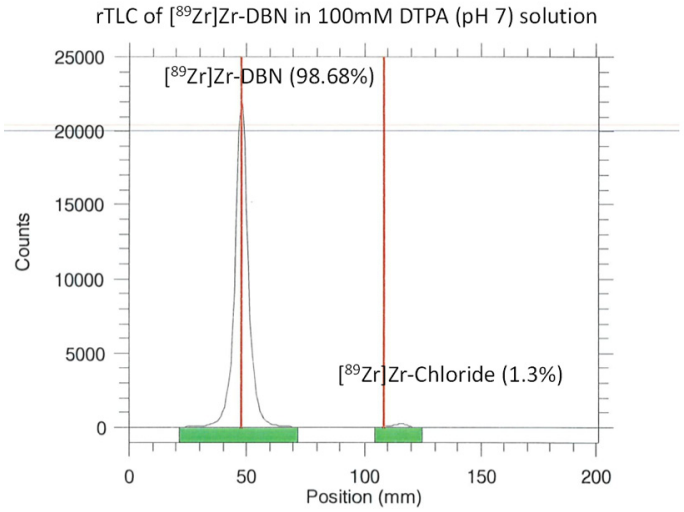

Reg	(mm) Start	(mm) Stop	(mm) Centroid	RF	Region Counts	Region CPM	% of Total	% of ROI
Rgn 1	21.1	72.2	48.0	0.000	177394.0	313048.2	97.91	98.68
Rgn 2	104.6	125.0	114.8	1.113	2374.0	4189.4	1.31	1.32
2 Peaks					179768.0	317237.6	99.22	100.00

Figure S1. rTLC of [89Zr]Zr-DBN in 100mM DTPA (pH 7) solution.

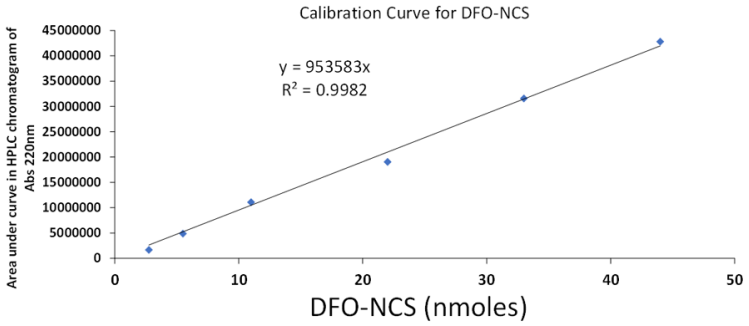

Figure S2. Concentration calibration curve for DFO-NCS.

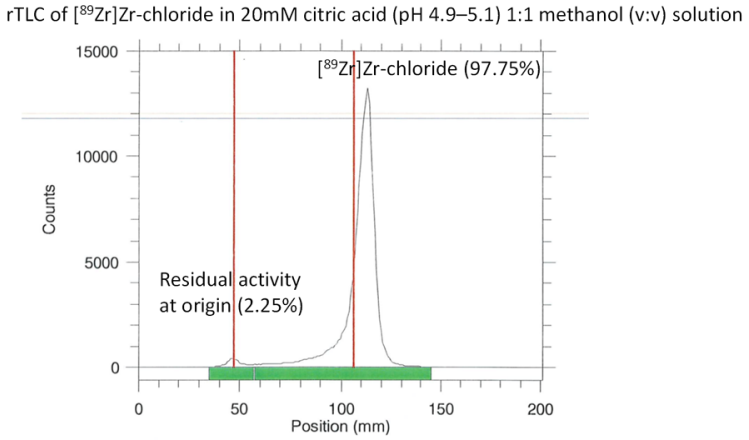

Reg	(mm) Start	(mm) Stop	(mm) Centroid	RF	Region Counts	Region CPM	% of Total	% of ROI
Rgn 1	34.7	56.9	47.5	0.008	4142.0	11296.4	2.24	2.25
Rgn 2	57.7	145.5	109.0	1.051	179776.0	490298.2	97.38	97.75
2 Peaks					183918.0	501594.5	99.63	100.00

Figure S3. rTLC of [89Zr]Zr-chloride in 20 mM citric acid (pH 4.9-5.1) 1:1 methanol (v:v) solution.

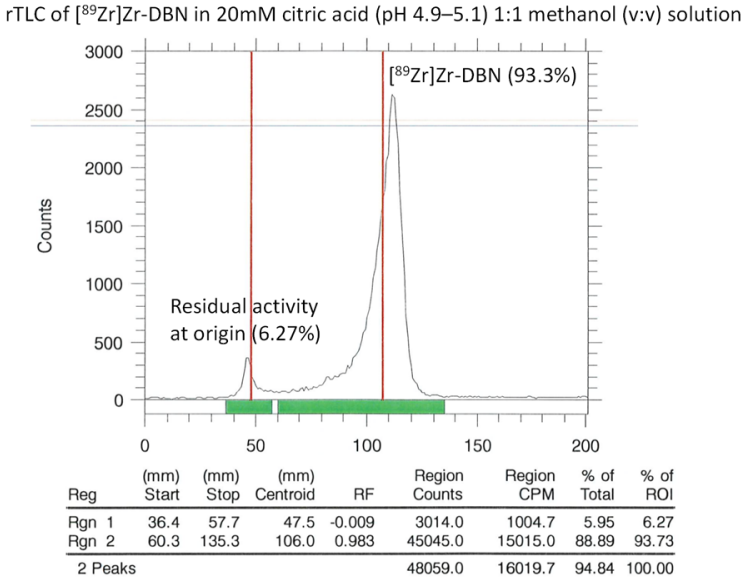

Reg	(mm) Start	(mm) Stop	(mm) Centroid	RF	Region Counts	Region CPM	% of Total	% of ROI
Rgn 1	36.4	57.7	47.5	-0.009	3014.0	1004.7	5.95	6.27
Rgn 2	60.3	135.3	106.0	0.983	45045.0	15015.0	88.89	93.73
2 Peaks					48059.0	16019.7	94.84	100.00

Figure S4. rTLC of [89Zr]Zr-DBN in 20 mM citric acid (pH 4.9-5.1) 1:1 methanol (v:v) solution.

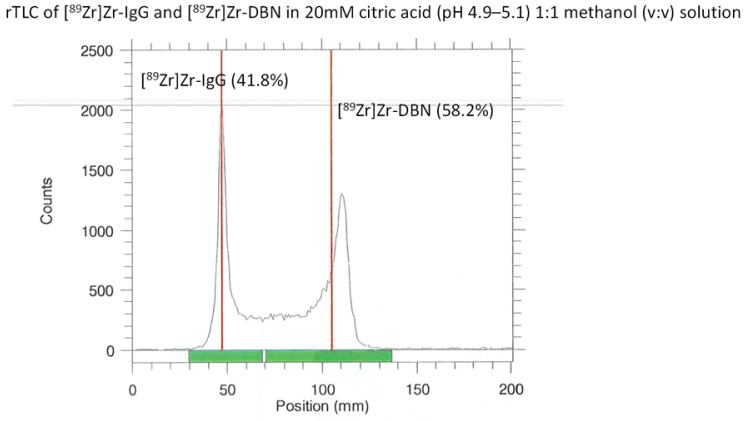

Reg	(mm) Start	(mm) Stop	(mm) Centroid	RF	Region Counts	Region CPM	% of Total	% of ROI
Rgn 1	29.6	68.8	50.7	0.063	19291.0	6430.3	40.60	41.83
Rgn 2	70.5	137.0	100.1	0.916	26826.0	8942.0	56.46	58.17
2 Peaks					46117.0	15372.3	97.06	100.00

Figure S5. rTLC of [89Zr]Zr-IgG and [89Zr]Zr-DBN in 20 mM citric acid (pH 4.9-5.1) 1:1 methanol (v:v) solution.

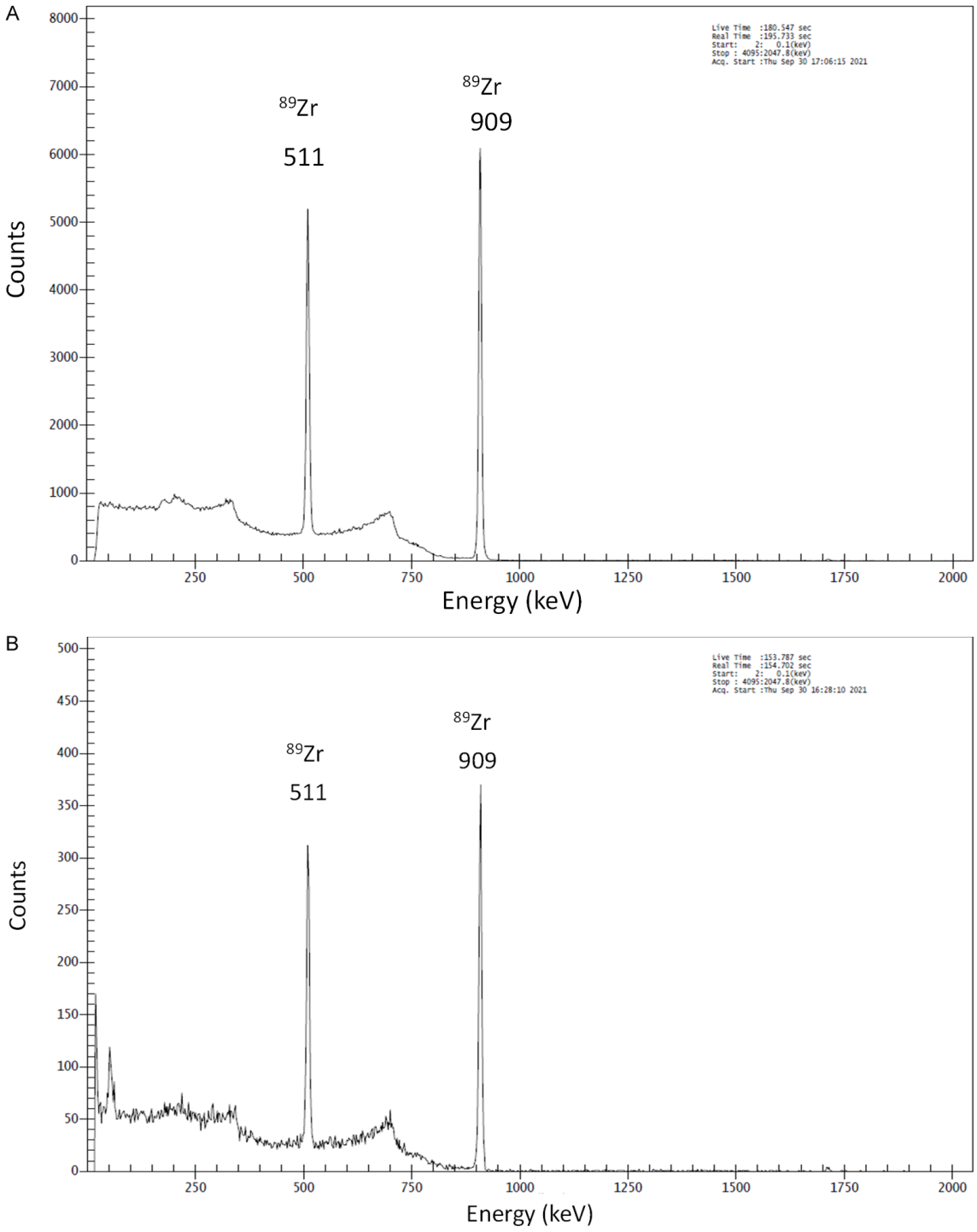
A
Live Time :180.547 sec
Real Time :195.733 sec
Start: 2: 0.1(keV)
Stop : 4095:2047.8(keV)
Acq. Start :Thu Sep 30 17:06:15 2021
^{89}Zr
511
^{89}Zr
909
Counts
Energy (keV)
B
Live Time :153.787 sec
Real Time :154.702 sec
Start: 2: 0.1(keV)
Stop : 4095:2047.8(keV)
Acq. Start :Thu Sep 30 16:28:10 2021
^{89}Zr
511
^{89}Zr
909
Counts
Energy (keV)

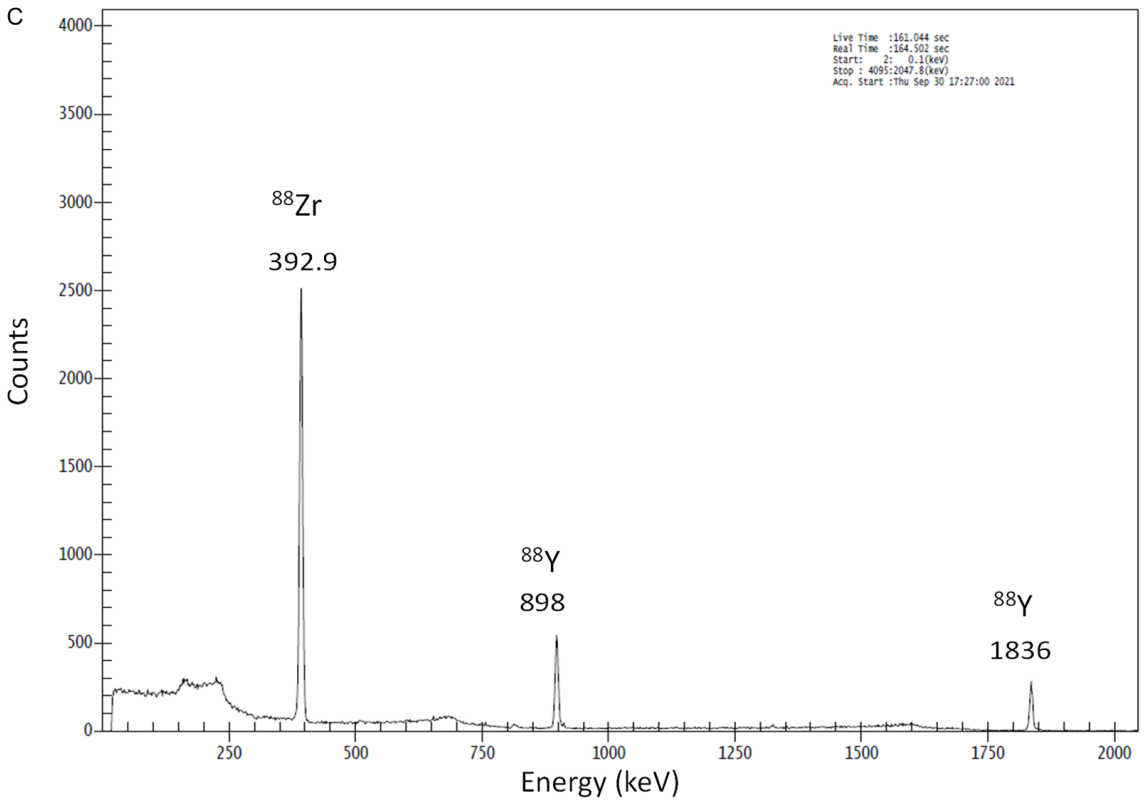

Figure S6. A-C: HPGe spectrums of ^{89}Zr produced at timepoint ^{88}Zr and ^{88}Y. A: HPGe spectrum of ^{89}Zr. B: HPGe spectrum of ^{89}Zr 60 days after the EOB. C: HPGe spectrum of ^{89}Zr 96 days after the EOB (produced at 15.2 MeV beam energy).

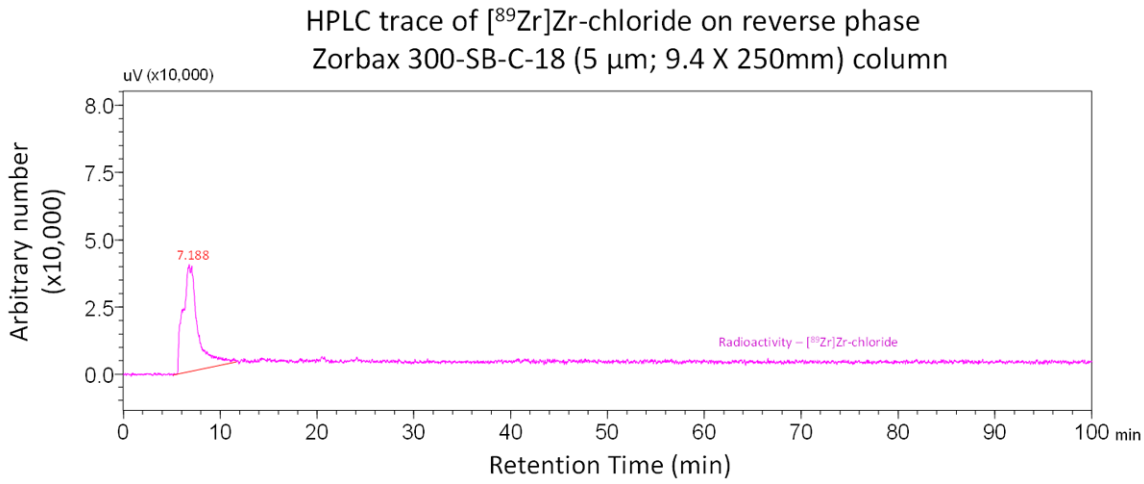

Figure S7. HPLC trace of [^{89}Zr]Zr-chloride.